



Si segregation deters prenucleation at the interfaces between liquid-aluminum and TiB₂ substrates, the origin of ‘Si poisoning’

Changming Fang^{*}, Yun Wang, Zhongyun Fan

Brunel Centre of Advanced Solidification Technology (BCAST), Brunel University London, Uxbridge, Middlesex, UB8 3PH, UK

ARTICLE INFO

Keywords:

Si poisoning
Al-Ti-B grain refinement
L-Al/TiB₂ interface
Prenucleation
Ab initio molecular dynamics

ABSTRACT

The mechanism of ‘Si poisoning’ of Al-Ti-B based grain-refiners in Al-Si alloys has been a topic of intensive study for over half a century. We here investigate prenucleation of Al at the Si segregated interfaces between liquid Al and TiB₂{0001} substrates using *ab initio* techniques. Our study reveals that chemical affinity between Ti and Si atoms empowers Si segregation at the Al(l)/substrate interface during solidification. The Si interfacial segregation curbs atomic ordering in the liquid Al adjacent to the substrate. Consequently, prenucleation of Al atoms at the Al(l)/{0001}TiB₂ interface is deteriorated and thus, the subsequent nucleation process adversely affected, which causes the so-called ‘Si poisoning’ effect during the practice of grain refinement via inoculation with addition of TiB₂ particles in Al-Si alloys.

In the early 1950s, Cibula and co-workers added Ti and B into liquid Al alloy for improving the mechanical performance of cast Al alloys via grain refinement [1]. Nowadays, grain-refiners such as the Al-*n*Ti-B (*n* = 3, 5) master alloys are widely used in Al industry [2,3]. The mechanisms of the grain refinement through inoculation with the grain-refiners have been a topic of intensive study for several decades for interests of both academic curiosity and industrial application [2–4]. Recently high-resolution scanning transmission electron microscopy (HR-STEM) revealed the formation of a Ti-rich two-dimensional compound (2DC), most likely Al₃Ti covering the TiB₂{0001} substrates in the cast Al samples [5]. This 2DC layer is believed to be responsible for the enhancement of potency of the TiB₂ particles to nucleate solid Al.

Atomic ordering in the liquid close to a liquid-metal/solid-substrate interface at a temperature higher than the nucleation point of the alloy is referred to as prenucleation [6,7]. It provides the essential precursor for the following nucleation and grain initiation [6,8]. Prenucleation is thus related to the intrinsic capability/potency of the substrate to nucleate a solid. Knowledge about chemical interactions between the atoms and prenucleation at a liquid/substrate interface is essential therefore, to obtain insight into solidification processes and the microstructures of the cast products.

Si in Al alloys deters grain refinement efficiency of Al-Ti-B grain-refiners. This effect is referred to as ‘Si poisoning’ [2,9–12]. Previous experiments have repeatedly found that low Si contents in Al-Si alloys have little impact on the Al-Ti-B grain refinement. However, when Si

content is more than 3wt.% in a hypoeutectic Al-Si alloy, the grain refinement via addition of the refiners is weakened and even deteriorated, with the grain size of α-Al increasing with Si concentration.

Existence of Si is inevitable in commercial Al metals/alloys and even more in Al scrap. As an essential alloying element, Si addition to Al alloys facilitates castability during solidification. Al-Si alloys/parts exhibit excellent mechanical performance and corrosion resistance, finding wide applications even under extreme conditions [2,13]. Currently, Al-Si-based alloys with 4wt% to 22wt% Si comprise majority (about 90%) of commercial Al alloy products [14]. It is thus, desirable to obtain high-Si content alloys of fine microstructures through inoculation with Al-Ti-B grain-refiners. For this purpose, knowledge about prenucleation and chemical interaction at the interfaces between liquid Al and TiB₂ substrates with Si segregation is crucial.

Both experimental and theoretical efforts have been made to understand the Si poisoning of the Al-Ti-B grain-refiners during solidification of Al alloys [9–13]. Recent experiments have focused on the local structure and chemical composition at the interfaces using HR-(S)TEM techniques. It has been revealed that Si atoms are enriched in the Al layer adjacent to the interfaces, resulting in the formation of a two-dimensional Al-Si alloy on the {0001} basal surface of the TiB₂ substrates [11,12]. First-principles methods have been employed to study the chemical bonding at the solid-Al/TiB₂ interfaces [15]. *Ab initio* molecular dynamics simulations (AIMD) were performed to investigate atomic ordering at the pristine interfaces between liquid Al and TiB₂ or

^{*} Corresponding author.

E-mail address: changming.fang@brunel.ac.uk (C. Fang).

Al_3Ti [16,17], and ‘Zr poisoning’ of the Al-Ti-B grain-refiners [18]. Meanwhile, there is still a lack about the origin of Si segregation and the subsequent effect on prenucleation at the interfaces between liquid Al and TiB_2 particles. Here we investigate prenucleation at the interface between liquid-Al and the $\text{TiB}_2\{0001\}$ (L-Al/ $\text{TiB}_2\{0001\}$ in short) with Si segregation using an AIMD technique. First-principles calculations and thermodynamics analysis are performed for Al $\{111\}$ / $\text{TiB}_2\{0001\}$ interfaces with Si segregation based on the recent experimental results [11,12].

For the AIMD simulations, a large hexagonal supercell with $a = 6a_0$ was used, where a_0 is the length of the a -axis of the TiB_2 unit cell with consideration of the thermal expansions of this ceramic material and Al at the simulation temperature [19,20]. Thus, a supercell with $a = 18.34 \text{ \AA}$ and $c = 43.52 \text{ \AA}$ was built for the (Si segregated) L-Al/ $\text{TiB}_2\{0001\}$ interfaces. It contains 828 atoms in total. A hexagonal supercell with a $2a_0 \times 2a_0$ in plane area was built for first-principles calculations of the Al $\{111\}$ / $\text{TiB}_2\{0001\}$ interfaces with Si segregation. A plane wave approach implanted in the first-principles code VASP [21] using the density-functional theory within the projector-augmented wave scheme [22] was employed. The generalized gradient approximation was employed to describe the exchange and correlation terms [23]. The AIMD simulations utilize the NVT ensemble [21] and the details are described in the Supplementary Materials. The snapshots for the equilibrated pristine (with no Si segregation) L-Al/ $\text{TiB}_2\{0001\}$ and the Si segregated interfaces are shown in Fig. 1a and c, respectively.

Ti and B atoms in TiB_2 substrate are well ordered, while the Al atoms far away from the substrate display little ordering, being liquid-like (Fig. 1). The Al(Si) atoms adjacent to the substrates exhibit density variation along the direction perpendicular to the substrates, which phenomenon is referred to as atomic layering that can be assessed by means of atomic density profile [7,24]. The layering at the pristine and the Si segregated L-Al/ $\text{TiB}_2\{0001\}$ interfaces was analyzed for configurations over 3 picoseconds (ps). The results are plotted in Fig. 1b.

Fig. 1a and b confirm pronounced layering of the liquid Al atoms close to the pristine L-Al/ $\text{TiB}_2\{0001\}$ interface. There are six recognizable layers, with the peak height decreases with the distance from the substrate. This is in good agreement with the previous AIMD simulations [7,16]. Moreover, Al atoms at the 1st Al layer are well separated from the atoms in neighboring layers (Fig. 1a).

At the equilibrated Si segregated Al/ TiB_2 interfaces, Si atoms are found to be positioned at the lower part of the first Al/Si layer (Fig. 1b and c). The peak height of the Si segregated layer is lower than the corresponding one at the pristine interface (Fig. 1b). There are only four recognizable layers (black curve in Fig. 1b) for the liquid atoms close to

the Si segregated interface. A close examination of Fig. 1b revealed an extra shoulder at about 0.4 \AA away from the 3rd Al peak at the Si segregated interface and the center of the 4th peak is about 0.5 \AA away from the one at the pristine interface. Layering of the liquid atoms close to the TiB_2 substrate at the Si segregated L-Al/ $\text{TiB}_2\{0001\}$ interface is clearly reduced as compared with that at the pristine interface.

The epitaxial nucleation model indicates a layer-by-layer growth of solid [6,25] during heterogeneous nucleation. The atomic arrangements in the liquid layers adjacent to the substrates determine the following nucleation process during solidification. Here the behavior of the liquid atoms adjacent to the substrates with and without Si segregation was analyzed. The time-averaged atomic arrangements (over 3 ps) at each atomic layer are shown in Fig. 2a–g. Moreover, the in-plane ordering coefficients [7,24] were employed to assess the atomic ordering in their respective layers near the interfaces. The results for configurations over 3 ps are plotted in Fig. 2h.

Fig. 2 shows that, at both interfaces, the termination Ti atoms of TiB_2 (Fig. 2a and d) are well ordered and strongly localized, being solid-like. This agrees with the high stability of the TiB_2 substrate. However, the in-plane atomic ordering of the liquid decreases with the layers away from the interfaces (Fig. 2h). At the pristine interface the 1st and 2nd Al layers show highly ordering and localization. Even the Al atoms in the 4th layer (Fig. 2g and h) show some contents of ordering and localization. In contrast, at the Si segregated interface the 1st Al(Si) layer shows delocalization (Fig. 2e) and the 2nd Al layer is already more liquid-like (Fig. 2f). The modelling unveils that the Si interfacial segregation significantly reduces the prenucleation at the Si segregated interface.

Fig. 2i shows the ratio of atom numbers of each Al(Si) layer to that of the well-ordered termination Ti layer (Fig. 2a, d). There is a notable difference in this ratio for the 1st Al(Si) layer at the interfaces. The 1st Al layer at the pristine L-Al/ $\text{TiB}_2\{0001\}$ interface has the $n(\text{Al})/n(\text{Ti})$ ratio = 1.01, whereas the $n(\text{Al,Si})/n(\text{Ti})$ ratio of the 1st layer at the Si segregated interface is as high as 1.13. This is unusual since the volume of a Si atom ($20.0 \text{ \AA}^3/\text{Si}$) in Si bulk is larger than that of an Al atom ($16.6 \text{ \AA}^3/\text{Al}$) [20]. The number of Al atoms in the 2nd layer increases little at the pristine interface, with the ratio being 1.02 which is lower than that at the Si segregated interface ($n(\text{Al})/n(\text{Ti})$ ratio = 1.07). In the 3rd layer, the number of Al atoms at the pristine system is the same as that at the Si segregated interface (1.08), close to the ratio of areas (1.08) between that of the $\text{TiB}_2\{0001\}$ substrate ($9.2 \text{ \AA}^2/\text{surface}$ at 1000 K [19]) and that of Al $\{111\}$ ($8.5 \text{ \AA}^2/\text{surface}$) at melting point [20]).

We further performed electronic structure calculations for the Si segregated L-Al/ $\text{TiB}_2\{0001\}$ system to get a deeper insight into the interfacial interactions. Based on the obtained electron density

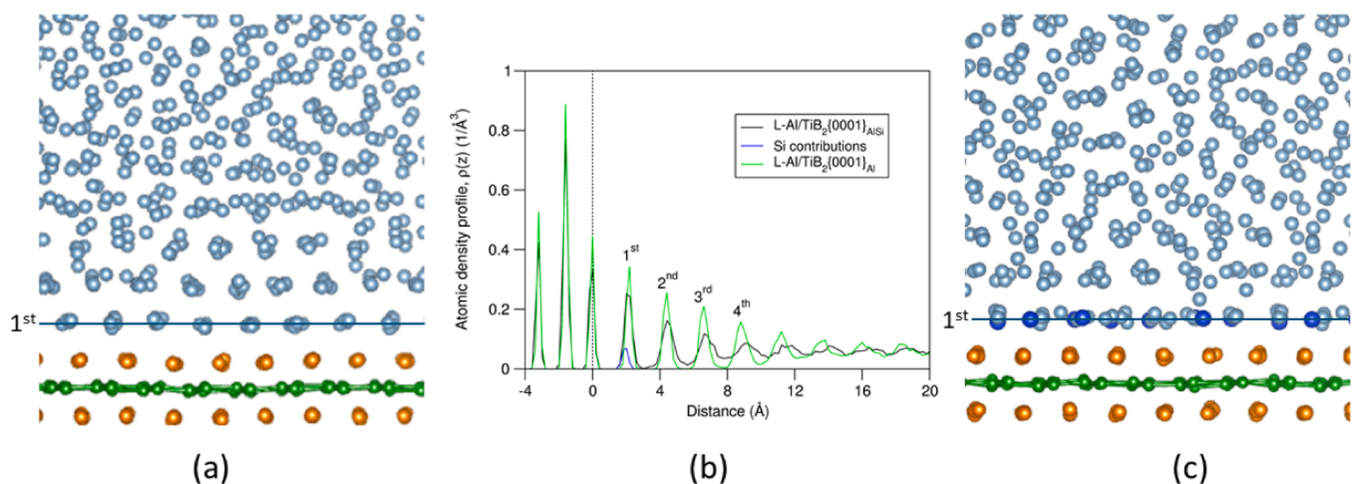


Fig. 1. Snapshots of pristine L-Al/ $\text{TiB}_2\{0001\}_{\text{Al}}$ (a) and Si segregated L-Al/ $\text{TiB}_2\{0001\}_{\text{AlSi}}$ interfaces (c) equilibrated at 1000K . Fig. 1b shows the atomic density files for the pristine L-Al/ $\text{TiB}_2\{0001\}$ (green curve), the Si segregated one (black curve) and the segregated Si atoms (blue curve). The vertical dotted line at 0 \AA represents the terminating Ti layer in (b). In 1a and 1c, the orange spheres represent Ti, small green B, silvery Al and blue Si.

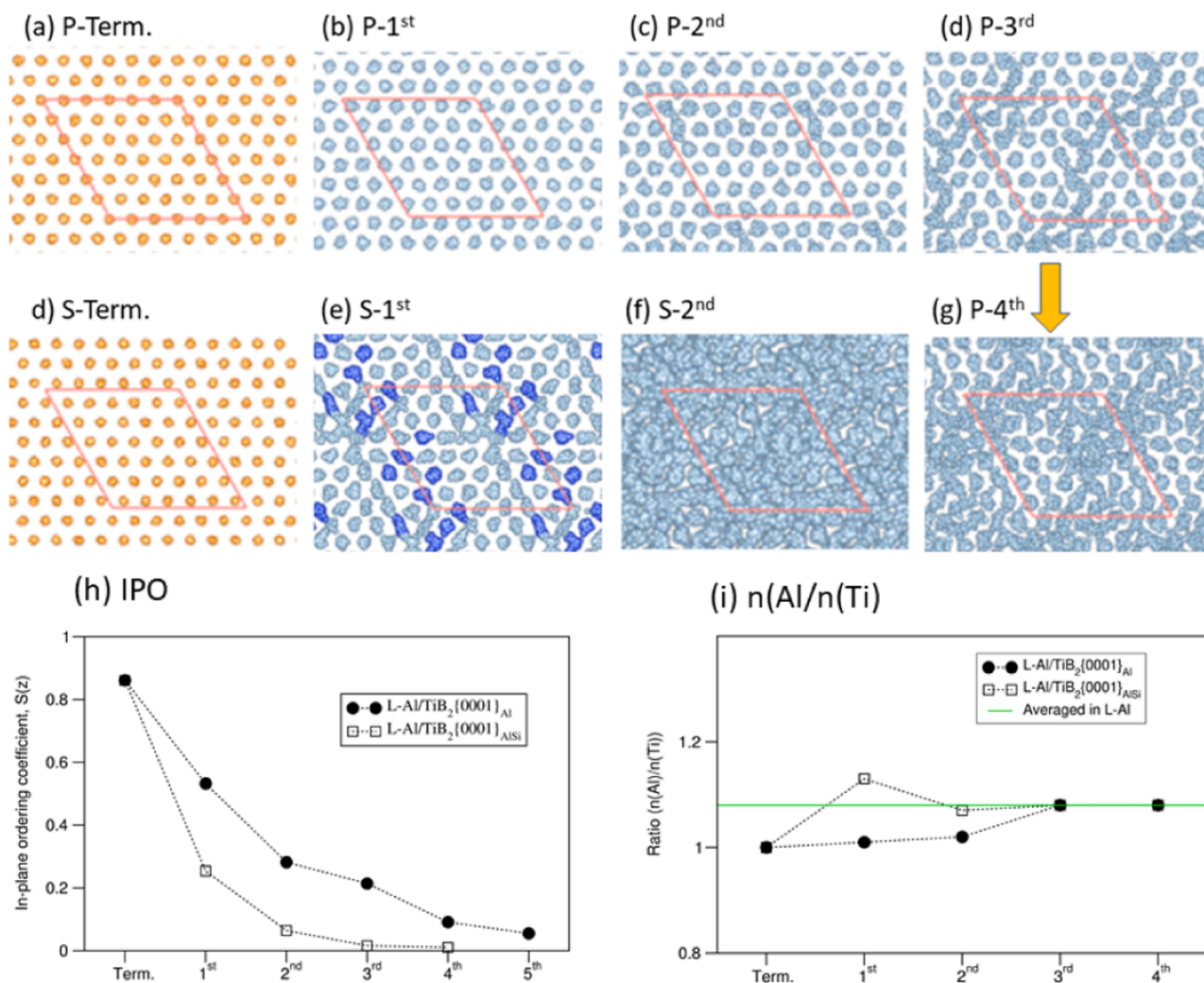


Fig. 2. The atomic arrangements summed for 3 ps at the layers nearby the interfaces for the pristine l-Al/TiB₂{00 01}_{Al} interface: (a) P-Term represents the terminating Ti layer, (b) P-1st the 1st Al layer, (c) P-2nd the 2nd Al layer, (d) P-3rd the 3rd Al layer and (g) P-4th the 4th Al layer; and the Si segregated l-Al/TiB₂{0001}_{AlSi} interface: (d) S-Term the terminating Ti layer, (e) S-1st the 1st Al layer and (f) S-2nd the 2nd Al layer. The in-plane ordering coefficients for both interfaces are plotted in (h) and the ratios of the atomic numbers in each layer to that of the termination Ti layer are shown in (i). The orange spheres represent Ti in (a) and (d), silvery Al, and blue Si (e). The red-lines represent the in-plane axis of the hexagonal lattice. The dotted lines in (h) and (i) are used to guide the readers' eyes.

distributions in Fig. 3a, the charges at the atomic sites at the interface were obtained via the Bader charge model [26,27] and the values are plotted in Fig. 3b.

Fig. 3a shows low electron densities around the naked Al ions away from the substrates. This corresponds to the free-electron nature of Al. Meanwhile, the Si atoms are surrounded by electrons and are negatively charged ($-0.3e/\text{Si}$ on average, Fig. 3b). The Al atoms away from the substrate are in fact electronically neutral. High electron densities are around B atoms and analysis showed that each B atom gains $0.5e/\text{B}$ on average. Meanwhile each Ti atom in the substrate is positively charged ($+1.0e/\text{Ti}$ on average). The termination Ti atoms lose $+0.7e/\text{Ti}$, of which $0.5e/\text{Ti}$ goes to B and $0.2e/\text{Ti}$ to the nearby Si and Al atoms. This corresponds to the lower electronegativity value of Ti (1.54 in Pauling scale) than those of Si (1.90) and Al (1.61).

High electron densities are found between the Ti and Si spheres, relating to the Si-Ti bonding (Fig. 3a). Such strong Si-Ti interaction corresponds to the high heat of mixing between Si and Ti (-66kJ/mol) compared with those between Al and Si (-19kJ/mol) and Al and Ti (-30kJ/mol) [28]. This is also reflected in the atomic density profiles that the Si atoms are closer to Ti as compared with the Al atoms in the same layer (Fig. 1). The attraction of Si ions to Al results in the increased

number of (Al+Si) atoms in the 1st metal layer at the Si segregated interfaces (Fig. 2i).

As shown in Fig. 1a at 1000 K, the liquid Al metal layers adjacent to the interface exhibit layering and in-plane ordering. Because of high energy cost for a Si atom in Al matrix [29], Si atoms in the layers would be forced to move away from the ordered Al layers to positions of lower potentials, e.g. being closer to Ti atoms. To get a deeper insight into the interfacial Si-Ti interactions, we performed first-principles calculations for Si at the Al{111}/TiB₂{0001} interface.

The formation energy, ΔE is defined as:

$$\Delta E(\text{Al}_{1-x}\text{Si}_x/\text{TiB}_2) = E(\text{Al}_{1-x}\text{Si}_x/\text{TiB}_2) - \{E(\text{Al}/\text{TiB}_2) + x[E(\text{Si}) - E(\text{Al})]\} \quad (1)$$

where, $E(\text{Al}_{1-x}\text{Si}_x/\text{TiB}_2)$, $E(\text{Al}/\text{TiB}_2)$, $E(\text{Al})$ and $E(\text{Si})$ are, respectively the calculated total valence-electrons energies for the Si doped system ($\text{Al}_{1-x}\text{Si}_x/\text{TiB}_2$), the pristine Al{111}/TiB₂{0001} system, and elemental Al and Si solids. The calculated formation energies on the Si content at $T = 0\text{ K}$ and $P = 0\text{ Pa}$ are plotted in Fig. 4a. The formation energies with respect to Si solute in Al matrix were also included in Fig. 4a. Fig. 4b shows schematically the Al{111}/TiB₂{0001} interface with Si

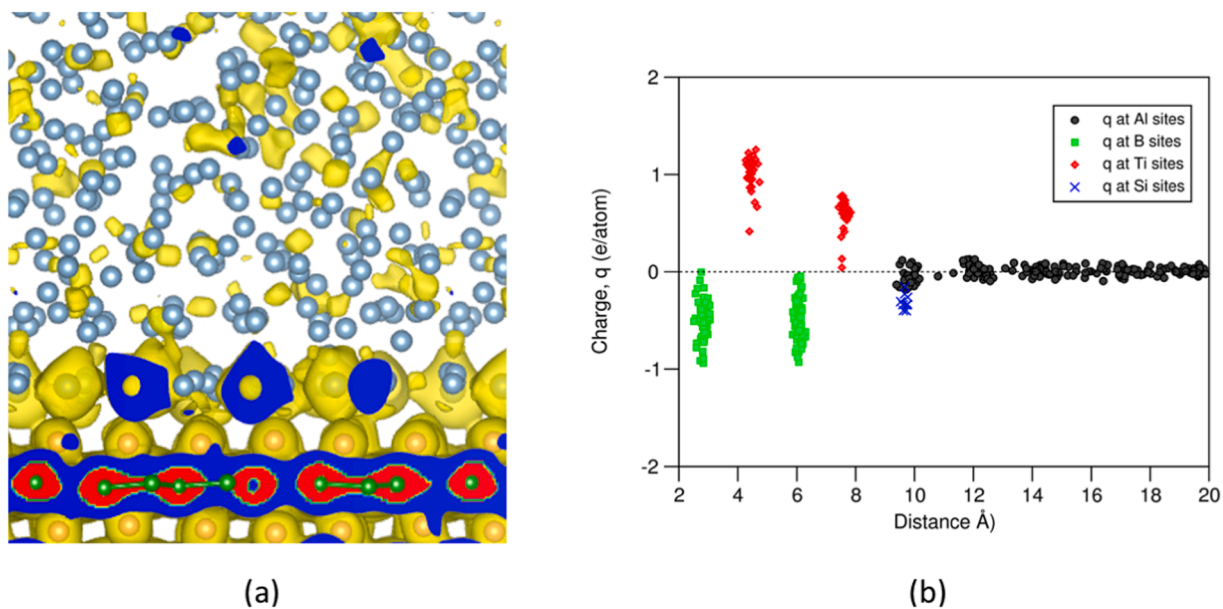


Fig. 3. (a) Iso-surfaces of the electron-density distributions ($\rho_0(r)=0.04e/\text{\AA}^3$) and (b) the Bader charges at the atomic sites for the Si segregated $1\text{-Al}/\text{TiB}_2\{0001\}_{\text{AlSi}}$ interface. In (a) the yellow spheres represent the isosurfaces, blue regions higher electron density, white lower electron density.

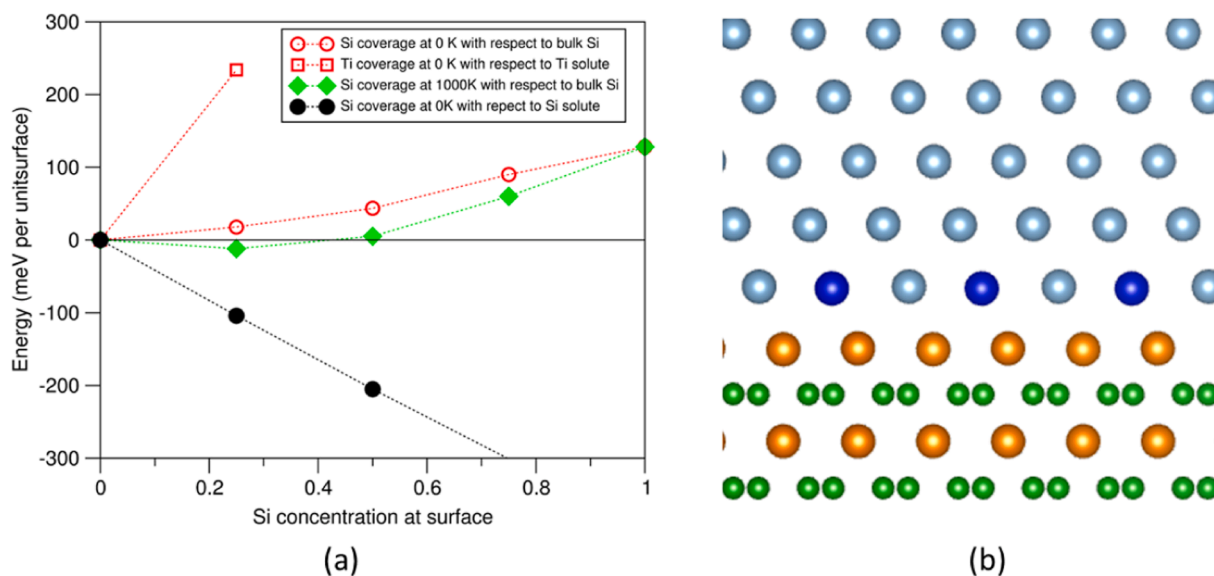


Fig. 4. (a) Dependences of the free energies of the Si segregated $\text{Al}\{111\}/\text{TiB}_2\{0001\}$ interface at 0 K with respect to bulk Si (unfilled red spheres) and solute Si (filled black spheres) on Si content at the 1st AlSi layer according to Equation 1. The green diamonds represent the free energies of Si segregated interface at 1000K. The energy of Ti segregation (red unfilled squares) is included for comparison. (b) A schematic structure of the Si segregated $\text{Al}\{111\}/\text{TiB}_2\{0001\}$ interface in which the green spheres represent B, silvery Al, orange Ti and blue Si. The dotted lines in (a) are used to guide readers' eyes.

segregation. Moreover, nucleation occurs at elevated temperatures, indicating contributions of the extra freedom for partial occupation of Si at the terminating layer to the free energy in stabilizing the system. The related Gibbs energy difference is, $\Delta G = \Delta H - T \Delta S$ and $\Delta S = R \ln w$, where w is the number of configurations in the random model, R the Boltzmann constant, ΔH the formation enthalpy, T the temperature, ΔS the configurational entropy. The obtained free energies with respect to bulk Si for the contents of Si atoms segregated at 1000 K is included in Fig. 4a.

Fig. 4a shows that at 0 K, replacement of one Al adjacent to the outmost Ti atoms by Si at the interface costs 18meV, which is significantly lower than the cost of replacement of one Al by Si in the Al matrix (430meV) [29]. This means that the Ti-Si interaction has strongly

reduced the energy cost of Si in Al. At the nucleation temperature (~ 933 K, the melting point of Al) the configurational entropy contribution stabilizes the Si segregations. The calculations showed that the favored Si content at the casting temperature is around 25 at.% with respect to bulk Si (green diamonds in Fig. 4a).

We also used Si solute in Al matrix as reference in Equation 1 (filled black spheres, Fig. 4a). With respect to Si solute in Al matrix Si segregation at the $1\text{-Al}/\text{TiB}_2\{0001\}$ is strongly favored even at 0 K, in well agreement with the experimental finding where Si segregation at Al/TiB₂ interface has been readily observed during casting [11,12].

During casting, with temperature decreasing the liquid Al atoms adjacent to the substrate become more ordered as shown in our AIMD simulations (Fig. 1) and in the literature [6,7]. The high energy cost of

solute Si in solid Al forces the Si adjacent to the TiB₂ substrate to move to lower potential positions. There are three possible sites for the Si atoms/ions to go: i) into the liquid; ii) to bulk Si nearby; and iii) to the layer adjacent to the TiB₂ substrates with Ti terminations. The first choice is suitable for most Si, especially for those away from the substrate. In this way these Si atoms become solute atoms in front of grain growth, which affects grain refinement according to [30], i.e., causing growth restriction. The second choice is most unlikely as the formation of Si bulk requires time and nuclei nearby. The last choice is likely for Si atoms close to the substrate, resulting in Si segregation at the l-Al/TiB₂ interface. The content of segregated Si atoms depends on the Si concentration in the liquid Al, i.e., the nominal Si concentration in a given Al-Si alloy. The segregated Si atoms may release the pre-existing Ti atoms in this layer (if there is any), reducing the nucleation potency of the TiB₂ substrates [5]. The limitation of segregation for Si in the liquid near the substrates also explains the experimental observations about the minimum Si content for ‘Si poisoning’ of the Al-Ti-B refiners in Al-Si alloys [11,12].

There are a rich variety of solid particles in alloys, e.g. MgO in Mg alloys, Al₃Ti and Al₂O₃ in Al alloys [6,16]. These particles may act as potential nucleation sites during solidification [6,16,17]. Recent experiments revealed segregation of impurities at oxide substrates [31], which modifies the nucleation potency of the substrates [32]. The mechanisms underlying the segregation of various impurities at the potential substrates and subsequent impacts on prenucleation deserve investigation for e.g. Al alloys scraps for recycling economy [33] and the present approach can be a useful tool.

CRedit authorship contribution statement

Changming Fang: Writing – review & editing, Writing – original draft, Visualization, Validation, Software, Resources, Project administration, Methodology, Investigation, Formal analysis, Data curation, Conceptualization. **Yun Wang:** Writing – review & editing. **Zhongyun Fan:** Writing – review & editing, Funding acquisition.

Declaration of interests

The authors declare that they have no known competing financial interests or personal relationships that could have appeared to influence the work reported in this paper.

Acknowledgment

Financial support from EPSRC (UK) under grant number EP/N007638/1 and EP/V011804/1 is gratefully acknowledged.

Supplementary materials

Supplementary material associated with this article can be found, in the online version, at [doi:10.1016/j.scriptamat.2024.116445](https://doi.org/10.1016/j.scriptamat.2024.116445).

References

- [1] A. Cibula, The grain refinement of aluminium alloy castings by addition of titanium and boron, *J. Inst. Metals* 80 (1951–1952) 1–16.
- [2] K.F. Kelton, A.L. Greer, *Nucleation in condensed matter: application in materials and biology*, Pergamon. Mater. Ser. (2010).
- [3] A.L. Greer, A.M. Buun, A. Tronche, P.V. Evans, D.J. Bristow, Modelling of inoculation of metallic melts: application to grain refinement of aluminium by Al-Ti-B, *Acta Mater.* 48 (2000) 2823–2835.
- [4] M.A. Easton, M. Qian, A. Prasad, D.H. StJohn, Recent advances in grain refinement of light metals and alloys, *Cur. Op. Solid State Mater. Sci.* 20 (2015) 13–24.
- [5] Z. Fan, Y. Wang, Y. Zhang, T. Qin, X.R. Zhou, G.E. Thompson, T. Pennycook, T. Hashimoto, Grain refining mechanism in Al/Al-Ti-B system, *Acta Mater.* 84 (2015) 292–304.
- [6] Z. Fan, Heterogeneous nucleation, grain initiation and grain refinement of Mg-alloys, in: Z. Fan, C. Mendis (Eds.), *Proc. The 11th international conference on magnesium alloys and their applications*, 24–27 July 2018, Beaumont Estate, Old Windsor, UK, 2018, p. 7. Ed. By.
- [7] C.M. Fang, H. Men, Z. Fan, Effect of substrate chemistry on prenucleation, *Metal. Mater. Trans. A* 49 (2018) 6231–4242.
- [8] Z. Fan, F. Gao, B. Jiang, Z.P. Que, Impeding nucleation for more significant grain refinement, *Sci. Rep.* 10 (2020) 9448.
- [9] M. Johansson, Influence of Si and Fe on the grain refinement of aluminium, *Z. Metallk.* 85 (1994) 781–785.
- [10] Y.C. Lee, A.K. Dahle, D.H. StJohn, J.E.C. Hutt, The effect of grain refinement and silicon content on grain formation in hypoeutectic Al-Si alloys, *Mater. Sci. Eng. A* 259 (1999) 43–52.
- [11] Y. Wang, Z.P. Que, T. Hashimoto, X.R. Zhou, Z. Fan, Mechanism for Si poisoning of Al-Ti-B grain refiners in Al alloys, *Metal. Mater. Trans. A* 51 (2020) 5743–5757.
- [12] J.H. Li, F.S. Hage, Q.M. Ramasse, P. Schumacher, The nucleation sequence of α -Al on TiB₂ particles in Al-Cu alloys, *Acta Mater.* 206 (2021) 116652.
- [13] Q. Cai, C.M. Fang, E. Lordan, Y. Wang, I.T.H. Chang and B. Cantor, A novel Al-Si-Ni-Fe near-eutectic alloy for applications at elevated temperatures, *Scripta Mater.* 237 (2023) 115707.
- [14] M.V. Glazoff, A.V. Khvan, V.S. Zolotarevsky, N.A. Belov, A.T. Dinsdale, *Casting Aluminum alloys, Their physical and Mechanical Metallurgy*, Butterworth-Heinemann (Elsevier), Oxford (UK)/Cambridge, MA (USA), 2019.
- [15] Y.F. Han, Y.B. Dai, D. Shu, J. Wang, B.D. Sun, First-principles calculations on the stability of Al/TiB₂ interface, *Appl. Phys. Lett.* 89 (2006) 144107.
- [16] J.S. Wang, A.P. Horsfield, U. Schwingenschlöggl, P.D. Lee, Heterogeneous nucleation of solid Al from the melt by TiB₂ and Al₃Ti: an *ab initio* molecular dynamics study, *Phys. Rev. B* 82 (2010) 184203.
- [17] D. Wearing, A.P. Horsfield, W.W. Xu, P.D. Lee, Which wets TiB₂ inoculant particles: Al or Al₃Ti? *J. Alloy. Compd.* 664 (2016) 460–468.
- [18] Y. Wang, C.M. Fang, L. Zhou, T. Hashimoto, X.R. Zhou, Q.M. Ramasse, Z. Fan, Zr poisoning of TiB₂ grain refinement, *Acta Mater.* 164 (2019) 428–439.
- [19] D. Yu Kovalev, N. Yu Khomenko, S.P. Shilkin, Thermal expansion of the nanocrystalline titanium diboride, *Ceram. Intern.* 48 (2022) 872–878.
- [20] J.W. Arblaster, *Selected Values of the Crystallographic Properties of the Elements*, ASM International, Materials Park, Ohio, USA, 2018.
- [21] G. Kresse, J. Furthmüller, Efficiency of *ab-initio* total energy calculations for metals and semiconductors using a plane-wave basis set, *Comp. Mater. Sci.* 6 (1996) 15–50.
- [22] P.E. Blöchl, Projector augmented-wave method, *Phys. Rev. B* 50 (1994) 17953–17978.
- [23] J.P. Perdew, K. Burke, M. Ernzerhof, Generalized gradient approximation made simple, *Phys. Rev. Lett.* 77 (1996) 3865–3868.
- [24] A. Hashibon, J. Adler, M.W. Finnis, W.D. Kaplan, Atomistic study of structural correlations at a liquid-solid interface, *Comp. Mater. Sci.* 24 (2002) 443–452.
- [25] Z. Fan, An epitaxial model for heterogeneous nucleation on potent substrates, *Metal. Mater. Trans. A* 44 (2013) 1409–1418.
- [26] R.F.W. Bader, A bonded path: a universal indicator of bonded interactions, *J. Phys. Chem. A* 102 (1998) 7314–7323.
- [27] G. Henkelman, A. Arnaldsson, H. Jónsson, A fast and robust algorithm for Bader decomposition of charge density, *Comp. Mater. Sci.* 36 (2006) 354–360.
- [28] A. Takeuchi, A. Inoue, Classification of bulk metallic glasses by atomic size difference, heat of mixing and period of constituent elements and its application to characterization of the main alloying element, *Mater. Trans.* 46 (2005) 2817–2829.
- [29] C.M. Fang, Z.P. Que, A. Dinsdale, Z. Fan, Si solution in θ -Al₁₃Fe₄ from first-principles, *Intermetallics* 126 (2020) 106939.
- [30] Z. Fan, F. Gao, Y. Wang, H. Men, L. Zhou, Effect of solutes on grain refinement, *Prog. Mater. Sci.* 123 (2022) 100809.
- [31] S.H. Wang, Y. Wang, Q.M. Ramasse, R. Schmid-Fetzer, Z.Y. Fan, Segregation of yttrium at the Mg/MgO interface in an Mg-0.5Y alloy, *Acta Mater.* 257 (2023) 119147.
- [32] C.M. Fang, Z. Fan, Effects of segregation of Sc, Y and La atoms on prenucleation at the l-Al/ γ -Al₂O₃ interfaces, *Metal. (Basel)* 12 (2022) 1550.
- [33] D. Raabe, et al., Making sustainable aluminum by recycling scrap: the science of ‘dirty’ alloys, *Prog. Mater. Sci.* 128 (2022) 100947.